Supporting Information

Tirapazamine-Assembled Phototherapy Agent for Combined Chemotherapy, Photodynamic Therapy, and Photothermal Therapy of Hepatocellular Carcinoma in Mice

Liang Chen,†[ab] Haiou Chen,†[b] Li Liu,[b] E Pang,[c] Yuanyu Tang,[c] Wei Ma,[d] Jierou Huang,*[e] Yongyin Li,*[a] Minhuan Lan *[c] and Yongjun Zhou *[af]

[a] Department of Infectious Diseases, Nanfang Hospital, Southern Medical University, Guangzhou, 510515, China; Key Laboratory of Infectious Diseases Research in South China (Southern Medical University), Ministry of Education

[b] Department of Infectious Diseases, Hunan Provincial People's Hospital, The First Affiliated Hospital of Hunan Normal University, Changsha, 410005, China

[c] College of Chemistry and Chemical Engineering, Central South University, Changsha, 410083, China

[d] Pu ai Medical School, Shaoyang University, Shaoyang, 422000, China

[e] Department of Rheumatology and Immunology, Hunan Provincial People's Hospital, The First Affiliated Hospital of Hunan Normal University, Changsha, 410005, China

[f] Hepatology Unit, Zengcheng Branch, Nanfang Hospital, Southern Medical University, Guangzhou, 511300, China

† Liang Chen and Haiou Chen contributed equally to this work.

* Corresponding authors.

E-mail address: huangjierou@hunnu.edu.cn (J, Huang), yongyinli@foxmail.com (Y. Li), minhuanlan@csu.edu.cn (M. Lan), zhou1991@smu.edu.cn (Y. Zhou)

Experimental Section

1. Materials and Reagents

Tirapazamine (TPZ) was obtained from Heowns Biochem Technologies, LLC (Tianjin, China). ITCC was obtained from Organtec Ltd. (Beijing, China). DSPE-PEG-NH_2-2000 was sourced from Shanghai ToYongBio Tech. Inc. (Shanghai, China). DMEM and PBS were obtained from Wuhan Servicebio Technology Co., Ltd. (Wuhan, China). Fetal bovine serum (FBS) was obtained from Nanjing Biochannel Biotechnology Co., Ltd. (Nanjing, China). Tetrahydrofuran (THF) and dimethyl sulfoxide (DMSO) were obtained from Shanghai Titan Scientific Co., Ltd. (Shanghai, China). 3-(4,5-Dimethylthiazol-2-yl)-2,5-diphenyltetrazolium bromide (MTT) was obtained from XienSi Biochemical Technology Co., Ltd. (Tianjin, China). Mitsubishi anaerobic gas-generating sachets (D-06/C-35) were purchased from Titan Scientific Co., Ltd. (Shanghai, China). Dialysis bags were obtained from Shanghai Yuanye Bio-Technology Co., Ltd. (Shanghai, China). Singlet Oxygen Sensor Green (SOSG) was obtained from Shanghai Maokang Biotechnology Co., Ltd. (Shanghai, China). Dihydrorhodamine 123 (DHR 123) was obtained from Beijing BioLab Technology Co., Ltd. (Beijing, China). 2′,7′-Dichlorodihydrofluorescein diacetate (DCFH-DA) was purchased from Macklin Biochemical (Shanghai, China). The JC-1 mitochondrial membrane potential assay kit was purchased from Shanghai Yeasen Biotechnology Co., Ltd. (Shanghai, China). The mitochondrial permeability transition pore (mPTP) assay kit was obtained from Nanjing Jiancheng Bioengineering Institute (Nanjing, China). Anti-HIF-1α antibody and anti-γ-H2AX antibody were purchased from Wuhan Servicebio Technology Co., Ltd. (Wuhan, China). Methylene blue (MB), 4′,6-diamidino-2-phenylindole (DAPI), trypsin–EDTA, and other routine reagents were purchased from commercial suppliers and used as received.

2. Cell Line and Animals

Hepa1-6 cells were obtained from Wuhan Servicebio Technology Co., Ltd. (Wuhan, China). C57BL/6J mice were acquired from Hunan SJA Laboratory Animal Co., Ltd. (Changsha, China).

3. Instruments and Equipment

UV–vis absorption spectra were recorded using a UV–vis spectrophotometer (UV-2600, Shimadzu, Japan), and fluorescence spectra were collected using a fluorescence spectrophotometer (RF-6000, Shimadzu, Japan). The hydrodynamic size, polydispersity index (PDI), and zeta potential of nanoparticles were measured using a dynamic light scattering/ζ-potential analyzer (Brookhaven Instruments Corporation, USA). Scanning electron microscopy (SEM) images were acquired using a field-emission SEM (JSM-7610FPlus, JEOL Ltd., Japan). Fluorescence images of cultured cells and tumor tissues, as well as bright-field images of stained tissue sections, were obtained using an inverted fluorescence microscope (DMIL LED, Leica, Germany). An ultrasonic cleaner was obtained from Kunshan Ultrasonic Instruments Co., Ltd. (Kunshan, China). The infrared thermal imager was obtained from Fluke Shanghai Corporation (Shanghai, China), and the paperless temperature recorder was obtained from Hangzhou Meacon Automation Technology Co., Ltd. (Hangzhou, China). The 635 nm laser was obtained from Shanghai Xilong Optoelectronics Technology Co., Ltd. (Shanghai, China). MTT assay absorbance was quantified using a multimode microplate reader (Multiskan GO, Thermo Fisher Scientific, USA). A VILBER imaging system was obtained from VILBER LOURMAT Corp. (France).

4. Preparation of TPZ、ITCC NPs and TPZ@ITCC NPs solution

TPZ was dissolved in ultrapure water to prepare a TPZ stock solution, followed by sonication until complete dissolution. The stock solution was aliquoted, protected from light, and stored at 4 °C until use. For UV–vis calibration, TPZ working solutions were freshly prepared in ultrapure water by serial dilution of the TPZ stock.

ITCC (2.9 mg) and DSPE-PEG-NH2-2000 (5.8 mg) were dissolved in 1.0 mL of tetrahydrofuran (THF). The resulting mixture was gradually added to 20.0 mL of water

while being subjected to ultrasonic treatment. The solution was then transferred to a dialysis bag (MWCO = 3500 Da) to remove any excess DSPE-PEG-NH2-2000 and THF. The final aqueous solution of ITCC NPs was obtained and stored in the dark at 4 °C.

ITCC (2.88 mg), TPZ (3.56 mg), and DSPE-PEG-NH_2-2000 (40 mg) were co-dissolved in THF (2 mL). The organic phase was then introduced into ultrapure water under bath sonication to form a uniform dispersion. The resulting suspension was transferred into a dialysis bag (MWCO 3,500 Da) and dialyzed against ultrapure water to remove organic solvent and free small molecules, yielding TPZ@ITCC NPs.

5. Optical properties, morphology, and stability

UV–vis absorption and fluorescence. UV–vis spectra were recorded for ITCC NPs, TPZ, and TPZ@ITCC NPs to confirm co-assembly and optical retention. Fluorescence spectra were acquired under identical settings for comparison.

UV–vis calibration curves for ITCC NPs and TPZ. Standard solutions of ITCC NPs and TPZ at various concentrations were prepared in appropriate solvents, and UV–vis spectra were recorded. Calibration curves were obtained by plotting absorbance versus concentration at 265 and 656 nm for ITCC NPs, and at 265 nm for TPZ. Linear regression was performed, and the fitted equations were used to determine ITCC and TPZ concentrations in TPZ@ITCC NPs for subsequent experiments.

Encapsulation efficiency (EE) and drug loading (DL). The amounts of incorporated TPZ and ITCC in TPZ@ITCC NPs were calculated from the corresponding UV–vis calibration curves. EE and DL were then determined according to the following equations: EE (%) = (amount of drug incorporated into nanoparticles / amount of drug initially added) × 100%; DL (%) = (amount of drug incorporated into nanoparticles / total mass of drug-loaded nanoparticles) × 100%.

Morphology characterization. The morphology of TPZ@ITCC NPs was examined by SEM. An aliquot of the aqueous TPZ@ITCC NP dispersion was dropped onto a silicon wafer and allowed to dry at room temperature. After drying, images were acquired using SEM.

Dynamic light scattering (DLS) and zeta potential. The hydrodynamic diameter, polydispersity index (PDI), and zeta potential of TPZ@ITCC NPs were determined using a dynamic light scattering/ζ-potential analyzer. Before measurement, TPZ@ITCC NPs were dispersed in deionized water, and all measurements were performed at room temperature.

Photostability. Aqueous TPZ@ITCC NP solutions (3 μM, 2 mL) and methylene blue (MB) solution (3 μM, 2 mL) were irradiated with a 635 nm laser (1 W/cm²) for 10 min. UV–vis absorption spectra were recorded every 2 min. The normalized absorbance decay (A_t/A_0) was calculated at 655 nm for TPZ@ITCC NPs and at 664 nm for MB.

Storage stability. TPZ@ITCC NP dispersions (3 μM) were stored in the dark at 4 °C. UV–vis absorption spectra were recorded on days 1–7 to evaluate spectral stability during storage. The hydrodynamic size was also measured by DLS on days 1–7 to assess size stability during storage.

6. Photothermal performance

A 635 nm laser was used with a spot diameter of 1.0 cm (irradiation area 0.785 cm²) at a fixed laser-to-sample distance of 10 cm. For solution measurements, temperature was recorded using a thermocouple positioned 0.5 cm below the liquid surface near the solution center without contacting the tube wall.

Temperature elevation curves in solution. 1.0 mL of TPZ@ITCC NP dispersions (10 μM, 5 μM, 2.5 μM, 1.3 μM, 0 μM) were irradiated with a 635 nm laser (1 W/cm², 10 min), and temperatures were recorded using a thermocouple.

Photothermal cycling stability. 1.0 mL of TPZ@ITCC NPs solution (20 μM) was irradiated with a 635 nm laser (0.3 W/cm²) for 10 min. After the solution was cooled to room temperature, irradiation was continued for another 10 min. This cycle was repeated 5 times. The temperature of an MB solution (20 μM) was also measured under the same conditions for comparison.

Photothermal conversion efficiency (PCE). 1.0 mL of TPZ@ITCC NPs solution (5 μM) was subjected to a 635 nm laser at 0.5 W/cm², irradiated until a steady-state temperature

was reached, followed by natural cooling; A thermocouple was used to record the temperature variation of the solutions.

7. ROS generation in solution

Singlet oxygen ($^1O_2$). SOSG (1 μL, 5 mM) was added to 2.0 mL TPZ@ITCC NP solution (3 μM), followed by 635 nm laser irradiation (0.05 W/cm²). Fluorescence spectra were recorded every 5 s to quantify $^1O_2$ generation kinetics. A water control (SOSG in water) was measured under identical conditions. The $^1O_2$ quantum yield was estimated using a relative method with methylene blue (MB) as the reference photosensitizer ($\Phi\Delta$ = 52%) under identical irradiation conditions with absorbance correction.

Superoxide anion ($O_2^{-}\cdot$). DHR123 (1 μL, 1 mg mL^{-1}) was added to 2.0 mL TPZ@ITCC NP solution (3 μM) and irradiated with a 635 nm laser (0.05 W/cm²). Fluorescence spectra were recorded every 5 s. A water control (DHR123 in water) was measured under identical conditions.

8. Cell culture and in vitro assays

Cell culture. Hepa1-6 cells were cultured in DMEM supplemented with 10% FBS at 37 °C with 5% CO_2. Cells were passaged using 0.25% trypsin–EDTA as needed.

8.1. Cytotoxicity (MTT) under normoxia and hypoxia

Normoxia. Cells were seeded into two 96-well plates at a density of 2×10^4 cells per well and incubated for 24 h. Cells were then treated with TPZ@ITCC NPs at different concentrations (31.2 μM/5 μM, 15.6 μM/2.5 μM, 7.8 μM/1.3 μM, 3.9 μM/0.6 μM, 2.0 μM/0.3 μM, and 0 μM/0 μM; expressed as TPZ/ITCC) in DMEM. For dark cytotoxicity, cells were incubated for 20 h in the dark. For photo-induced cytotoxicity, cells were incubated for 4 h in the dark, irradiated (635 nm, 1 W/cm², 10 min), and then incubated for another 16 h in the dark. MTT working solution was then added and incubated for 4 h. After removing the medium, DMSO was added to dissolve formazan crystals, and absorbance was measured at 490 nm using a microplate reader.

Hypoxia. Cells were seeded into two 96-well plates at a density of 2×10^4 cells per well and incubated for 24 h. Cells were preconditioned in a hypoxia bag with an anaerobic gas-generating sachet for 2 h. The medium was then replaced with DMEM containing TPZ@ITCC NPs at the concentrations described above, and the hypoxic environment was maintained throughout the assay. Subsequent dark or laser treatments and the MTT readout were performed as described for normoxia, with all steps kept under hypoxic conditions where applicable.

8.2. Intracellular ROS detection

Hepa1-6 cells were assigned to four groups (n = 3 per group): PBS, PBS+L, TPZ@ITCC NPs, and TPZ@ITCC NPs+L, where 'L' denotes laser irradiation. Cells were seeded in 24-well plates and cultured to ~60% confluence, then treated with PBS or TPZ@ITCC NPs for 4 h. Cells were incubated with DCFH-DA in serum-free medium for 30 min at 37 °C in the dark, washed, and the indicated groups were irradiated (635 nm, 1 W/cm², 10 min). Cells were optionally counterstained with DAPI, and fluorescence was imaged using an inverted fluorescence microscope.

8.3. Mitochondrial membrane potential (Δψm) detection

Δψm was evaluated by JC-1 staining. Following the same grouping scheme as above, Hepa1-6 cells were seeded in 24-well plates and cultured to ~60% confluence, followed by the indicated treatments for 4 h. The groups requiring laser irradiation were then irradiated (635 nm, 1 W/cm^2, 10 min). Cells were washed twice with pre-warmed PBS and incubated with JC-1 staining solution (5 μg mL^{-1} in serum-free DMEM) at 37 °C for 20 min in the dark. Cells were rinsed twice using the JC-1 washing buffer and imaged by fluorescence microscopy. The green/red fluorescence intensity ratio was quantified with ImageJ; an increased ratio indicates mitochondrial depolarization.

8.4. Mitochondrial permeability transition pore (mPTP) opening assay

mPTP opening was assessed using a calcein-AM/$CoCl_2$ quenching assay. Following the same grouping scheme as in the Δψm assay, Hepa1-6 cells were treated with PBS or TPZ@ITCC NPs for 4 h, and the indicated groups were irradiated (635 nm, 1 W/cm², 10 min). Cells were then incubated with calcein-AM (1 μM) and $CoCl_2$ (1 mM) for 30 min in the dark, washed, and imaged by fluorescence microscopy. Reduced green

fluorescence indicates mPTP opening.

8.5. γ-H2AX immunofluorescence staining under hypoxia

Hepa1-6 cells were assigned to four groups (n = 3): PBS, PBS + L, TPZ@ITCC NPs, and TPZ@ITCC NPs + L, where "L" denotes laser irradiation. Cells were seeded in 24-well plates containing glass coverslips and cultured to approximately 60–70% confluence. To mimic hypoxic conditions, cells were pre-incubated in a hypoxia bag with an anaerobic gas-generating sachet for 2 h, and the subsequent treatment was carried out under hypoxia as much as possible, following the hypoxic treatment protocol described in Section 8.1. Cells were then treated with PBS or TPZ@ITCC NPs for 4 h. The indicated groups were exposed to 635 nm laser irradiation (1 W/cm², 10 min). After treatment, cells were washed with PBS, fixed with 4% paraformaldehyde for 15 min, permeabilized with 0.1% Triton X-100 for 10 min, and blocked with 5% BSA for 30 min at room temperature. Cells were then incubated with an anti-γ-H2AX primary antibody overnight at 4 °C, followed by incubation with the corresponding fluorescent secondary antibody for 1 h at room temperature in the dark. Cell nuclei were counterstained with DAPI, and fluorescence images were acquired using an inverted fluorescence microscope. The relative fluorescence intensity of γ-H2AX was quantified using ImageJ.

9. In vivo studies

All animal procedures were carried out in accordance with the Regulation on the Administration of Laboratory Animals (People's Republic of China) and the Chinese National Standards GB/T 35892-2018 and GB/T 35823-2018. This study is reported in accordance with the ARRIVE 2.0 guidelines. All procedures were approved by the Ethics Committee for Experimental Animal of The First Affiliated Hospital of Hunan Normal University (Approval No. 2024-146). Six-week-old C57BL/6J mice of either sex (vendor as described in "Cell Line and Animals") were housed under standard SPF conditions (22 ± 2 °C, 50–60% relative humidity, 12 h light/dark cycle) with ad libitum access to food and water and environmental enrichment. A subcutaneous hepatocellular carcinoma model was established by subcutaneously inoculating 1×10^6 Hepa1-6 cells

into the flank.

9.1. In vivo antitumor efficacy

When tumors reached ~100 mm^3, mice were randomly assigned to four groups: PBS, PBS+L, TPZ@ITCC NPs, and TPZ@ITCC NPs+L (n = 5 per group; total n = 20). In total, 100 μL of either PBS or TPZ@ITCC NPs (31.2 μM/5 μM, expressed as TPZ/ITCC) were injected intratumorally. After injection, mice in the PBS+L group and TPZ@ITCC NPs+L group were exposed to a 635 nm laser at 1 W/cm^2 for 10 min. Tumor length (a) and width (b) were measured with electronic calipers on days 0, 1, 3, 5, and 7 during treatment, and tumor volume was calculated as $V = a \times b^2 / 2$. Body weight was recorded concurrently. On day 7, mice were euthanized, and tumors were excised and weighed. The experimental unit was one mouse. Randomization was performed using a computer-generated random number sequence. No animals or data points were excluded from the analyses. Blinding was not performed during tumor measurement and endpoint assessment. The primary outcome measure was tumor volume; secondary outcomes included tumor weight and body weight. Cage positions were rotated regularly to minimise potential confounders. Animals were monitored at least once daily for general condition and tumor burden, and humane endpoints were predefined in the approved protocol (e.g., ulceration, impaired mobility, or excessive tumor burden). Euthanasia was performed by overdose of pentobarbital sodium, with death confirmed prior to tissue collection.

9.2. In vivo fluorescence imaging

After intratumoral injection, mice were imaged using a NIR fluorescence animal imaging system. Whole-body fluorescence imaging was performed after injection using a VILBER imaging system (λ_{ex} = 640 nm, λ_{em} = 670-720 nm) to assess in vivo biodistribution.

At predetermined time points (0, 12, 24, 36, and 48 h) after intratumoral injection of TPZ@ITCC NPs, mice were euthanized and the major organs, including the heart, liver, spleen, lung, and kidney, were harvested. Ex vivo fluorescence imaging of the isolated organs was then performed using the same VILBER imaging system (λex = 640 nm,

λem = 670–720 nm) to evaluate the time-dependent biodistribution and clearance behavior of the ITCC fluorescence signal.

9.3. Infrared thermal imaging

Mice in PBS + L and TPZ@ITCC NPs + L groups were exposed to a 635 nm laser at 1 W/cm^2 for 10 min. During irradiation, a thermal imager was used to capture their images, and the temperature changes at the tumor site in tumor-bearing mice were recorded.

9.4. Histology and blood analysis

After mice were euthanized, tumors and major organs (heart, liver, spleen, lung, kidney) were harvested. Tumors and organs were fixed, paraffin-embedded, sectioned, and subjected to H&E staining; tumor sections were further analyzed by Ki67 immunohistochemistry and TUNEL staining.

Blood was collected from the orbital venous plexus for complete blood count (WBC, RBC, HGB, PLT) and serum biochemistry (ALT, AST, CRE, CK) measurements.

9.5. HIF-1α and γ-H2AX immunofluorescence staining of tumor sections

Tumors were harvested at the study endpoint, fixed in 4% paraformaldehyde, paraffin-embedded, and sectioned. After deparaffinization and rehydration, sections were subjected to antigen retrieval, followed by blocking with 5% BSA at room temperature. Serial tumor sections were then incubated overnight at 4 °C with primary antibodies against HIF-1α or γ-H2AX, respectively. After washing with PBS, the sections were incubated with the corresponding fluorescent secondary antibodies for 1 h at room temperature in the dark. Nuclei were counterstained with DAPI. Fluorescence images were acquired using an inverted fluorescence microscope under identical imaging settings for all groups. The mean fluorescence intensities of HIF-1α and γ-H2AX were quantified using ImageJ.

10. Data analysis and statistics

Data are presented as mean ± SEM. For in vitro experiments, n denotes the number of independent biological replicates (independent cell samples/wells prepared and treated in parallel), unless otherwise stated; for in vivo experiments, n denotes the number of

mice per group. Statistical analyses were performed using GraphPad Prism (v8.0.2). Comparisons among multiple groups were conducted using one-way ANOVA followed by Tukey's multiple-comparisons post hoc test. Experiments involving two factors (e.g., treatment × time) were analyzed using two-way ANOVA followed by Sidak's multiple-comparisons post hoc test. Statistical significance was defined as *$p < 0.05$, **$p < 0.01$, and ***$p < 0.001$.

Supplementary Figures

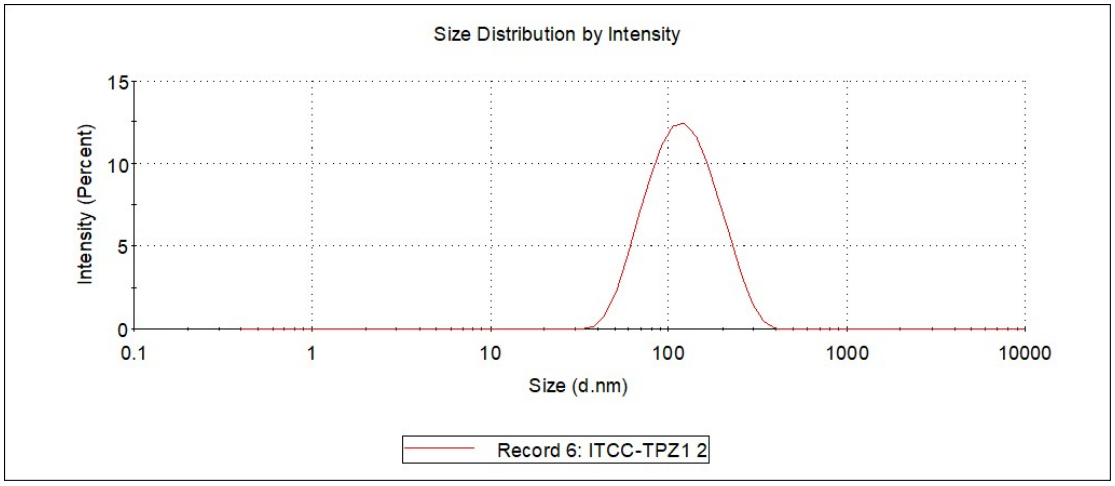

Figure S1. Hydrodynamic size distribution of TPZ@ITCC NPs measured by DLS in aqueous solution. The average hydrodynamic diameter was 101.3 nm and the PDI was 0.224.

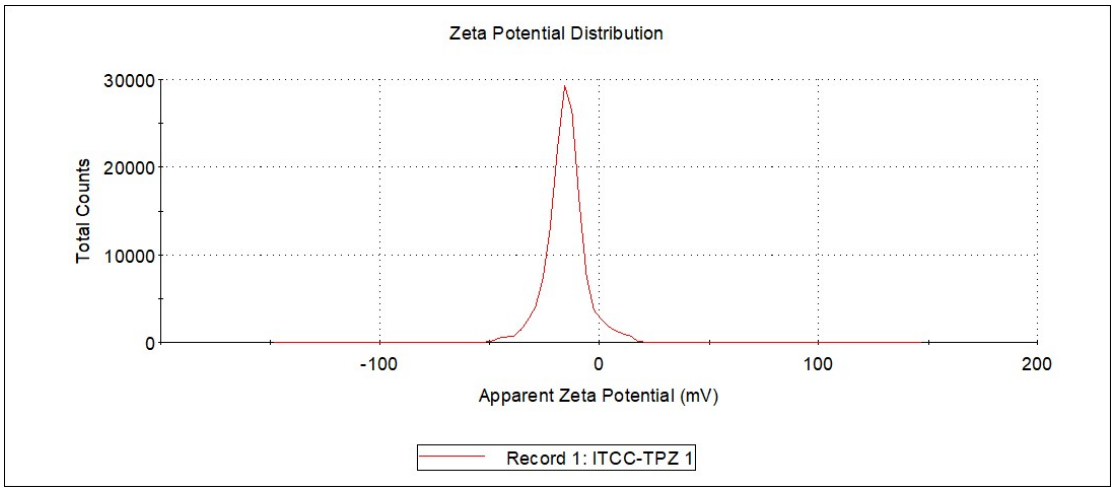

Figure S2. Zeta potential distribution of TPZ@ITCC NPs in aqueous solution. The measured zeta potential was -15.2 mV.

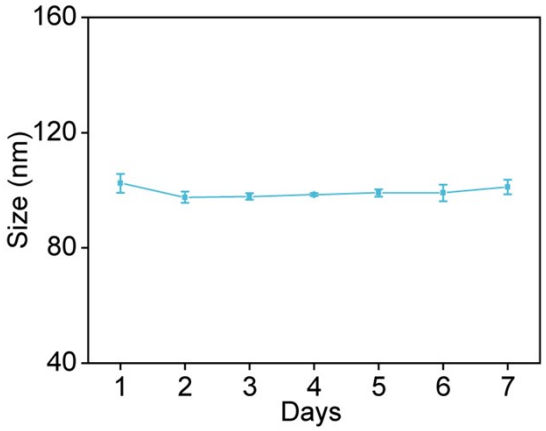

Figure S3. Hydrodynamic size changes of TPZ@ITCC NPs during storage for 7 days.

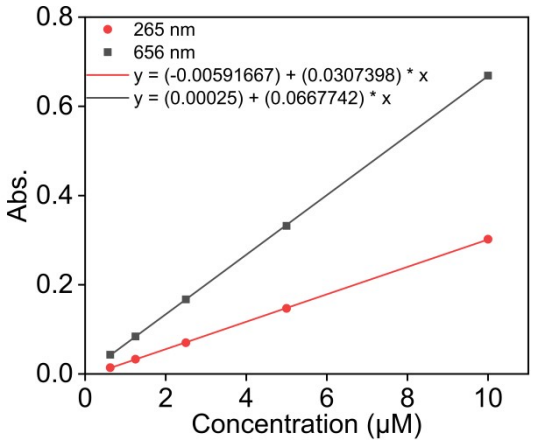

Figure S4. UV–vis calibration curves of ITCC NPs at 265 nm and 656 nm.

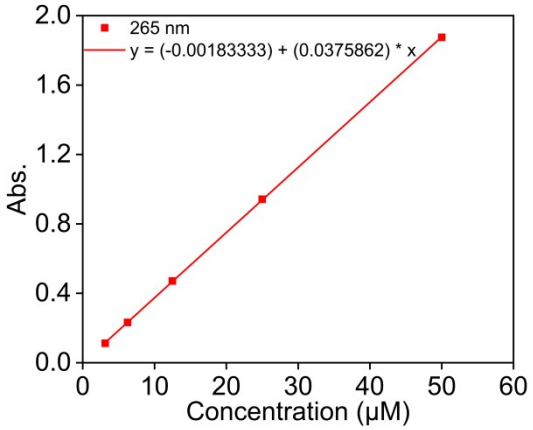

Figure S5. UV–vis calibration curve of TPZ at 265 nm.

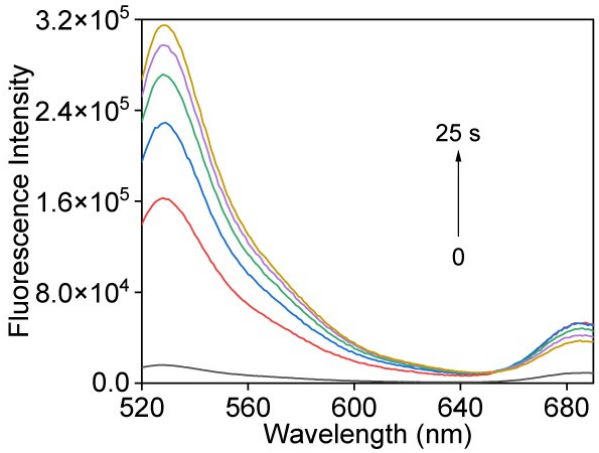

Figure S6. Fluorescence spectral changes of the reference photosensitizer methylene blue (MB) under 635 nm laser irradiation.

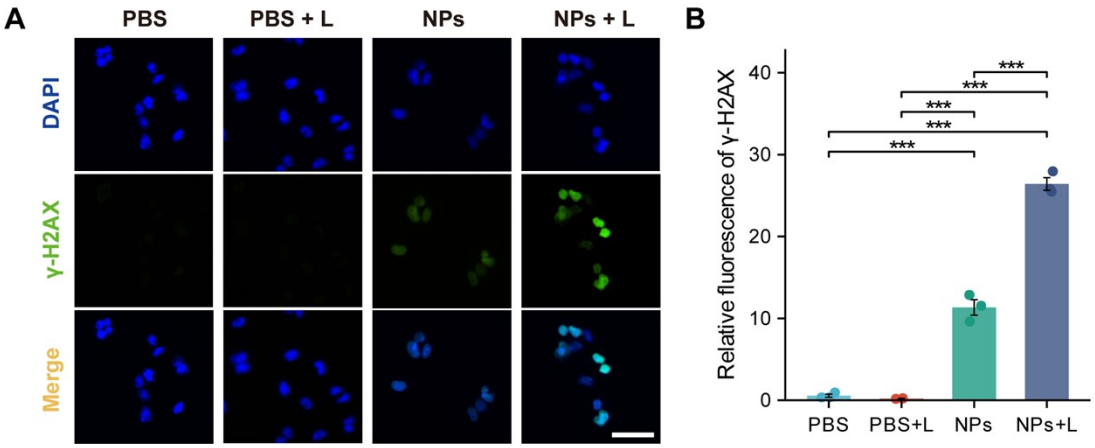

Figure S7. γ-H2AX immunofluorescence staining of Hepa1-6 cells after different treatments under hypoxic conditions. (A) Representative fluorescence images of γ-H2AX staining in Hepa1-6 cells after different treatments. Nuclei were counterstained with DAPI (blue), and γ-H2AX is shown in green. (B) Quantitative analysis of relative γ-H2AX fluorescence intensity. (Scale bar: 50 μm, n = 3).

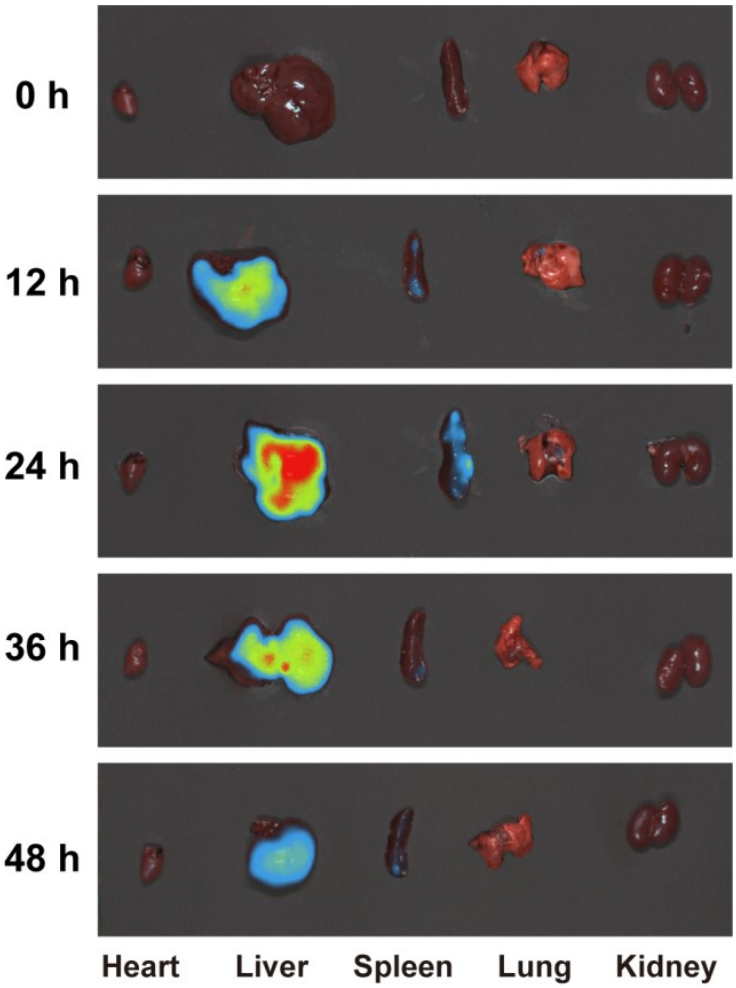

Figure S8. Ex vivo fluorescence imaging of major organs at different time points after intratumoral injection of TPZ@ITCC NPs.

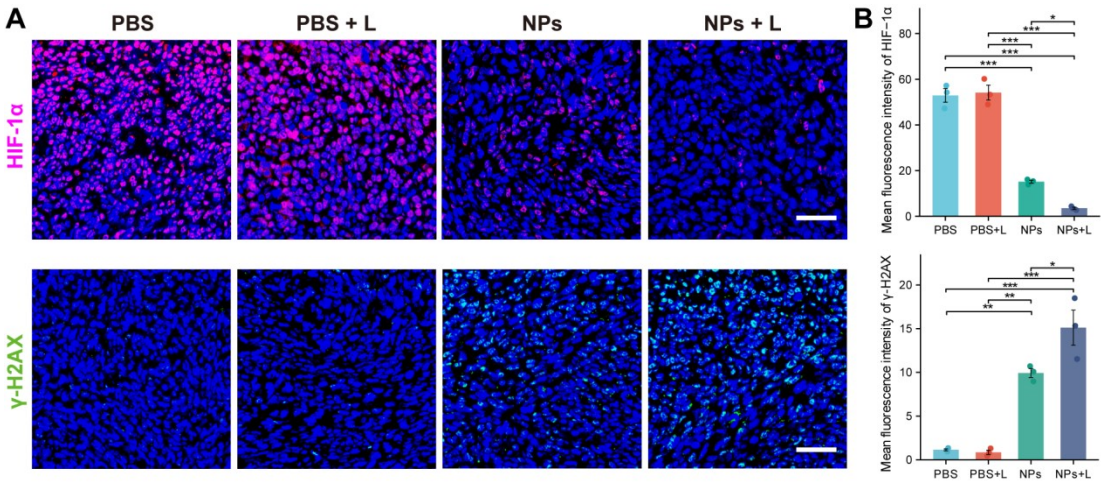

Figure S9. HIF-1α and γ-H2AX immunofluorescence staining of tumor sections after different treatments. (A) Representative immunofluorescence images of HIF-1α (upper row, magenta) and γ-H2AX (lower row, green) in tumor sections from the different

groups. Nuclei were counterstained with DAPI (blue). (B) Quantitative analysis of the mean fluorescence intensities of HIF-1α and γ-H2AX in tumor sections. (Scale bar: 50 μm, n = 3).